engineering proceedings

MDPI

Proceeding Paper

On the Compressive Behavior of Platonic- and Pacioli-Inspired Lattice Structures via FEA †

Carmine Martino [1,2], Chiara Bertolin [1], Francesco Penta [2,*] and Chao Gao [1]

[1] Department of Mechanical and Industrial Engineering, Norwegian University of Science and Technology (NTNU), 7034 Trondheim, Norway; carmi.martino@studenti.unina.it (C.M.); chiara.bertolin@ntnu.no (C.B.); chao.gao@ntnu.no (C.G.)
[2] Department of Industrial Engineering, Federico II University, 80134 Naples, Italy
* Correspondence: penta@unina.it
† Presented at the 53rd Conference of the Italian Scientific Society of Mechanical Engineering Design (AIAS 2024), Naples, Italy, 4–7 September 2024.

Abstract: Shapes and topologies of lattice materials have been extensively studied, yet very few studies have dealt with shapes inspired by ancient mathematicians, such as the Platonic solids discovered by Plato in 360 BC or the mathematical behavior of the unexplored "semi-regular" solids of Pacioli (1445–1517). Using the finite element analysis method, the buckling and post-buckling behavior of Platonic and Paciolian cells subjected to a compressive load were analyzed. In these solids, the energy absorbed per unit mass is an increasing function with the number of faces, similar to porosity, which reaches a maximum value for solids comprised of 90–100 surfaces.

Keywords: finite element analysis; cellular structures; strut-based lattices; mechanical properties; Platonic solids; Pacioli's solids

check for updates

Academic Editors: Umberto Galietti, Gabriele Arcidiacono, Enrico Armentani, Davide Castagnetti, Vigilio Fontanari, Aurelio Somà and Nicola Bonora

Published: 4 March 2025

Citation: Martino, C.; Bertolin, C.; Penta, F.; Gao, C. On the Compressive Behavior of Platonic- and Pacioli-Inspired Lattice Structures via FEA. *Eng. Proc.* **2025**, *85*, 33. https://doi.org/10.3390/engproc2025085033

Copyright: © 2025 by the authors. Licensee MDPI, Basel, Switzerland. This article is an open access article distributed under the terms and conditions of the Creative Commons Attribution (CC BY) license (https://creativecommons.org/licenses/by/4.0/).

1. Introduction

Periodic metamaterials embody a revolutionary category of materials engineered to exhibit exceptional properties that conventional materials cannot achieve. Among the broad class of metamaterials, periodic metamaterials consist of repeating unit cells arranged in a periodic lattice structure that, while having a design that is extremely lightweight, still offer high mechanical strength. For this reason, lattice materials are the last frontier of material mechanics. They are a new class of engineering materials with potential for use in a very wide range of applications, including structural biomedical implants [1–3], aerospace and naval structures [4], sports equipment [5], and photonic and phononic crystals [6,7].

Both the geometry of their unit cells and the material for their fabrication may be chosen to achieve very unusual properties, such as negative thermal expansion, negative Poisson's ratio, fluid-like elasticity, or high damping capacity. Mechanical engineers are continuously seeking new unit cell designs to enhance the efficiency of their properties and the lightness of their structures. Inspiration to develop new designs has been found in the past by looking at the geometries that past mathematicians have invented. In particular, our attention has been devoted to a group of five regular solids attributed to Plato (Athens 428/427 B.C.–Athens 348/347 B.C.) that have equal sides, equal faces, and are circumscribed by a sphere. They belong to a group of solids invented in the 15th century by the Italian mathematician Luca Pacioli (Borgo Sansepolcro 1445–Borgo Sansepolcro 1517) who evolved original Platonic geometries by discovering new solids through the work of Leonardo Da Vinci in *De Divina Proportione* (1509). In this paper, the properties of these fascinating solids

are explored. Further, recently developed geometries are proposed as potential new unitary cells for lattice materials.

Except for a limited number of studies [8–10], very few works have focused on the advantages offered by unit cells that have the fascinating regularity properties of Platonic solids. Unfortunately, there is still considerable controversy surrounding the responses of such cells' units under quasi-static compressive loading conditions. Additionally, the behavior of metamaterials that have unit cells with the "semi-regular" solid geometry proposed by Pacioli is still fully unexplored.

Nevertheless, the properties of these families of unit cells appear to be well-suited for use in the sacrificial components of passive safety devices and can be readily manufactured using modern additive technology, aligning with sustainable design principles for product recyclability and a circular economy.

In this paper, the results of an explorative study aimed at extending our current knowledge on the behavior of Platonic- and Pacioli-inspired strut-based unit cells are presented.

Specifically, a procedure for generating Pacioli-derived unit cells with a high number of faces is reported geometrically and analytically in Sections 2.1 and 2.2. Then, the buckling and post-buckling response of Platonic- and Pacioli-inspired cells under diametral compressive loading are analyzed by the finite element method (presented as a method in Section 2.3) in the Results Section (Section 3). The numerical results highlight that it is possible to create a new family of solids, with a compressive mechanical behavior that is dependent on the number of surfaces. It can be observed that the porosity of the solids increases as the number of surfaces increase and stabilizes around a maximum asymptote for solids with 90 to 100 surfaces. Also, the compressive mechanical behavior of the new family of solids improves with an increasing number of surfaces and they generally have better behavior than Platonic solids. The same happens with the energy absorbed per unit mass during compression, which shows improvement as the number of surfaces increases. That is, the solid with 100 surfaces is better at employing its material to absorb energy.

2. Methods

2.1. Geometrical Modelling

Since all the Platonic solids are inscribed in a sphere, it was essential for their realization in the CAD model to draw the sphere first, keeping the radius value constant for each solid.

For all solids, it was necessary to first draw the frame of the structure (see Figure 1, step 1), that is, the set of all sides. For this aim, the Platonic solids' basic property of equal faces and edges was exploited. Then, the size of the solid edges was a consequence of imposing the constraint of coincidence between the vertices and the sphere surface.

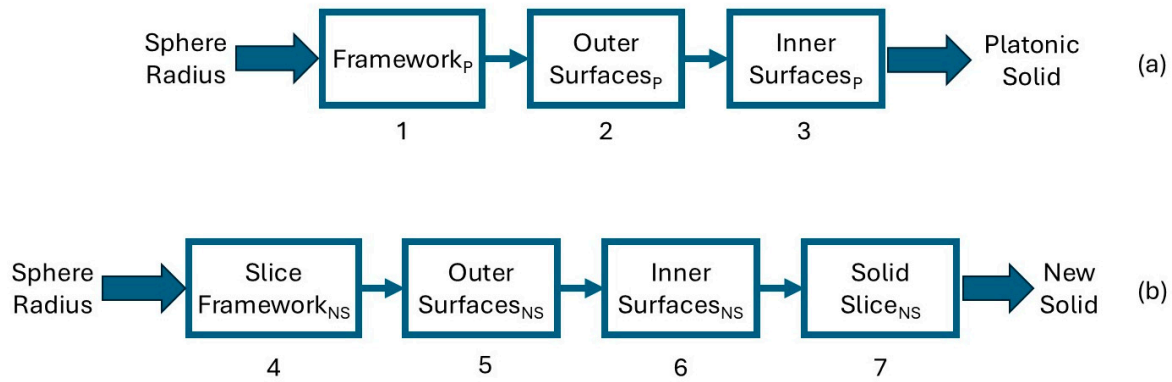
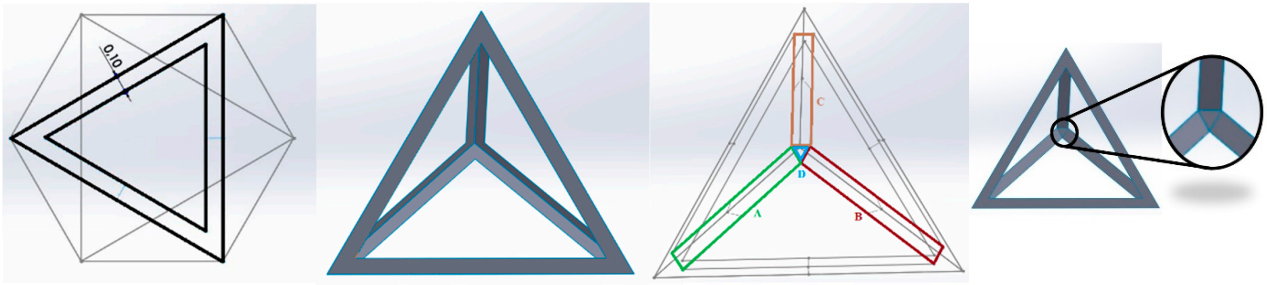


Figure 1. Representation of the methodological steps followed to realize the geometric models of (**a**) the Platonic solid; (**b**) the new Pacioli's solid. Subscript P = Platonic; Subscript NS = New Solid.

Therefore, once the line drawings of the frames of these structures are made (step 1, Figure 1a), a solid with its own volume can be identified. The solid can be fully filled or it can remain internally hollow to be represented as a lattice structure.

To draw the lattice structure of a solid, it was decided to start fixing the lattice size measured on the faces' plane. Then, in each face, the inner profile of the external surfaces was created by offsetting the faces' edges at a distance equal to the chosen thickness, as shown in Figure 2a.



(**a**) (**b**) (**c**) (**d**)

Figure 2. Illustration of (**a**) application of the offset from the outer perimeter for the construction of the latex surface; (**b**) solid built with external surfaces only; (**c**) joining of vertices for the creation of surfaces in the third dimension inside the solid; (**d**) solid as shown in (**b**) but zoomed in on the intersections of four inner surfaces.

As shown in Figure 2b, only the surface profile of the external surfaces for each face is visible. However, to have the third dimension inside the solid, a profile for the internal surfaces has to be created using the 3D sketch function by joining all internal vertices appropriately (i.e., Figure 2c), thus obtaining the final solid as shown in Figure 2d.

The decision to use all planar faces was crucial because as the thickness varied, the external bulk should not have exceeded the volume of the sphere where the solid under examination was inscribed.

Following the same methodology, all five Platonic solids were modelled.

In the book published in 1509 by Luca Pacioli, it is possible to find the Leonardo drawings of the Pacioli semi-regular solids in both monolithic (volume filled) and reticular (lattice structure) form. In the CAD environment, only the following 15 solids were realized: *Tetraedron Absci svs*, *Tetraedron Eleu tvs*, *Hexiedron Abscisvs*, *Hexaedron Elevatum*, *Hexaedron Siue Cubus Abfcifum Eleuatum*, *Octaedron Abfcifum*, *Octaedron Eleuatum*, *Icosaedron abscisus*, *Icosaedron Eleuatum*, *Dodecaedron Abfcifum*, *Dodecahedron Elevatum*, *Dodecaedron Abfcifum Eleuatum*, *Vigintisex basium Planum*, *Vigintisex Basium Eleuatum*, and *Septuaginta duarum Basium*. They were chosen due to their suitability for further analysis.

In particular, among the selected solids, the attention was focused on the solid *Septuaginta Duarum Basium (SDB)* due to its cyclic symmetry properties. Furthermore, this solid is inscribable in a sphere, it is convex, and its geometry can be easily modified to increase the number of faces, thus realizing new geometries.

The structure of this solid has a circular symmetry, with the slices being repeated twelve times. In addition, there are six faces for each slice, with the upper three mirroring the lower three in relation to the equatorial plane of the solid. Only by changing the number of circular repetitions can a different number of surfaces can be obtained. Since each slice in SDB has six faces, each time the number of slices is changed, another solid is obtained with the number of faces equal to an integer multiple of six. As this was a limiting factor, the structure was modified to a meridian curve to have more flexibility. A polygonal chain of five segments was arranged symmetrically with respect to the equatorial plane of the cell in order to have a family of faces of the solid parallel to the axis of the cell. Regarding

the length of these segments, it was decided to make their projections equal on the axis of the solid so that wall rods of greater length were on the edges of the faces farthest from the equatorial plane. A cell frame slice was obtained by drawing two such polygonal chains on two meridian planes that were rotated from each other by the angle

$$\theta = \frac{360^\circ}{\eta}, \tag{1}$$

where η is the number of cell slices. Then, the slice frame was completed by drawing the segments joining the chains' vertices that belonged to the same planes normal to the cell axis (Figure 1, step 4).

For the transition from frame to lattice solid, identical steps were followed as those shown for Platonic solids (Figure 1, steps 5 and 6). This method was then repeated cyclically for the required number of times (Figure 1 step 7). Following this method, the number of planar faces delimiting the solid can be increased (by five at a time) by increasing the number of segments or "slices" that make up the solid, keeping in mind that at least three segments are required to obtain the solid.

2.2. Mathematical Modelling

Lattice materials differ from monolithic materials essentially because of the internal porosity that has been quantified for each solid in terms of the normalized porosity index ΔV_R given by

$$\Delta V_R = \frac{\Delta V}{V_S}, \tag{2}$$

where

$$\Delta V = V_m - V_L \tag{3}$$

is the difference between the monolithic volume solid V_m and the lattice solid volume V_L, while

$$V_S = \frac{4}{3}\pi R^3 \tag{4}$$

is the volume of the circumscribed sphere.

The ΔV_R values were plotted as a function of the number of solid faces in Figure 3b. They were evaluated for the case of lattice solids having the maximum possible lattice thickness, as shown in Figure 3a.

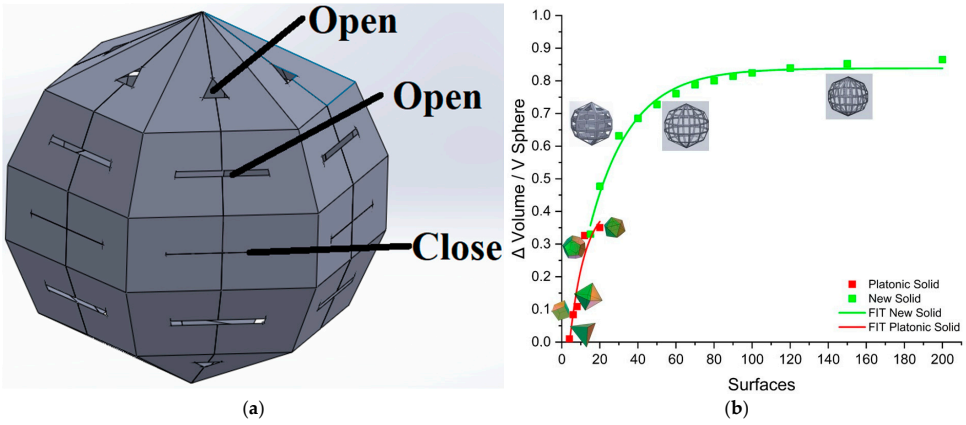


Figure 3. (**a**) Cell of lattice material with maximum thickness with only the central surfaces closed; (**b**) Plot values of ΔV_R versus the number of surfaces of the representative solids.

As a further step, the dimensions of the bounding box, namely a parallelepiped, that contains and delimits the dimensions of the solid, were assessed. It was possible to obtain

the dimensions of the new solids with CAD. For the Platonic solids, an attempt was made to evaluate them mathematically as a function of the radius of the circumscribed sphere alone.

2.3. Finite Element Method Modelling

Once the unit cells' geometries were designed, the buckling and post-buckling properties of the examined cells were studied using the finite element method (FEM).

The lattice structure of each cell, constructed with sizes circumscribed by a sphere of radius R = 50 mm, was discretized using Euler beam elements (B31) in a commercial FEM environment (Abaqus CAE). For the sake of simplicity, it was assumed that all the beams of a cell had circular cross sections with a diameter equal to 8.0 mm and that they were made of polylactic acid (PLA), a material extensively used in fused deposition modeling (FDM) technology.

The mechanical properties of PLA were taken from [11] and listed in Table 1 below.

Table 1. Properties of PLA extracted by [11].

Material Property	Value	Units
Elastic modulus (E)	3149	MPa
Poisson's ratio (υ)	0.36	-
Yield strenght (σ_y)	77	MPa

The average size of the elements was equal to 4 mm. The FE model cell had a number of nodes that varied between 4 (for the tetrahedron cell) and 82 (for the 100-surface cell).

Preliminarily, for each cell, an eigenvalue buckling analysis was carried out to identify the critical valuesof the self-equilibrated compressive loads that were applied along the radial direction of the circumscribed sphere using a couple of cell nodes that were diametrically opposite. Adopting this procedure, the cell orientation was such that the loading direction was aligned with the vertical z-direction of the global reference frame. Moreover, all the translational and rotational degrees of freedom (DOF) of the cell's lowest node were restrained.

The first five eigenvalues and the corresponding eigenvectors of each cell were calculated for such loading conditions (see Table 2 in the Section 3).

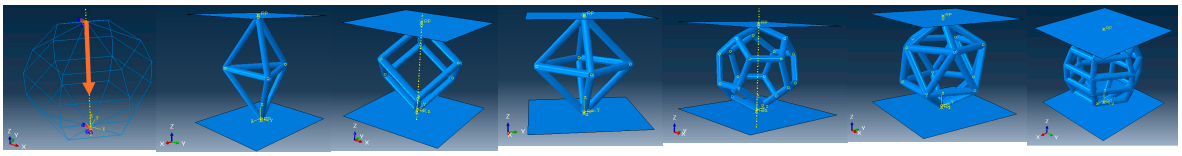
Table 2. Eigenvalue of all solids in buckling analysis.

Solid	Eigen Value
Tetrahedron	4639.4
Cube	4625.4
Octahedron	6462.3
Dodecahedron	8870.1
Icosahedron	9615.7
30 Surface	13,506
60 Surface	28,951
100 Surface	50,146

Post-buckling properties of each cell were examined simulating a compressive test between rigid plates in the FEM environment. To activate the cell buckling mode in this analysis, the critically deformed shapes corresponding to the lowest eigenvalue of the preliminary buckling analysis, after suitably scaling, were adopted as initial geometrical imperfections.

The mechanical behavior of the cell material in the post-buckling study was assumed to be linear–elastic and ideally plastic without hardening. Also, in this case, constitutive properties of the PLA material listed in Table 1 were adopted.

FE cell models were initially located between two rigid plates, oriented in the global cartesian reference frame and constrained in the same way as the buckling analysis, as shown in Figure 4b–g. The plates were both normal to the *z*-axis and were adopted to simulate the actions of the support plate and the punch of the testing machine on the cell. Therefore, the lowest one was fixed and in the same horizontal plane as the constrained node of the cell. The other one was initially at a distance slightly greater than 2*R from the fixed plate. Gradually increasing displacements along the z-direction were applied to the unit cell while all the other rigid DOF were locked. The interactions of the cell with both plates were modeled by the *node to surface contact* subroutine. Cell nodes were chosen as master nodes while plate elements were adopted as target surfaces. To speed up the simulations, it was chosen to neglect—in this explorative study—interactions between cell elements caused by strut deformations. For this reason, simulations were stopped as soon as the contact between cell elements was detected.



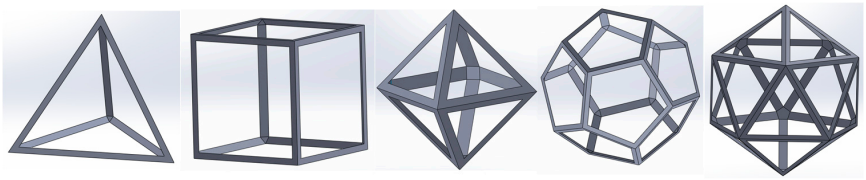
(**a**) (**b**) (**c**) (**d**) (**e**) (**f**) (**g**)

Figure 4. Representation of solids in the AbaqusCAE environment: (**a**) 30-surface solid with axial force (orange arrow) for buckling analysis; (**b**) tetrahedron representation between rigid plates for post-buckling analysis; (**c**) cube; (**d**) octahedron; (**e**) dodecahedron; (**f**) icosahedron; (**g**) 30-surface solid.

3. Results

3.1. Geometrical Modelling Results

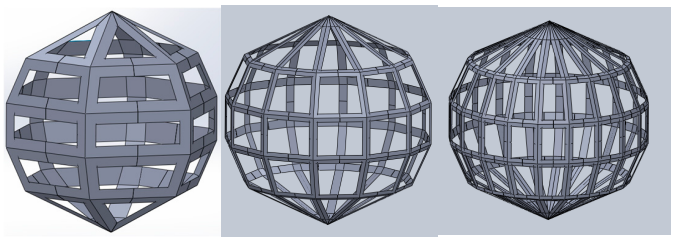
Within the framework of Platonic solids, the five solids drawn and reported in Figure 5 were the following: *tetrahedron*, *cube*, *octahedron*, *dodecahedron*, *icosahedron*. They were drawn as lattice materials; therefore, they were characterized by having a frame and a certain characteristic thickness with an internal empty space.



(**a**) (**b**) (**c**) (**d**) (**e**)

Figure 5. Representation of the elementary cells of latex Platonic solids, realized in 3D CAD environment: (**a**) tetrahedron; (**b**) cube; (**c**) octahedron; (**d**) dodecahedron; (**e**) icosahedron.

Then, new solids were created as solids with 30, 60, and 100 surfaces (Figure 6).



(**a**) (**b**) (**c**)

Figure 6. Representation of the elementary cells of the new solid lattice, realized in 3D CAD environment: (**a**) 30 surfaces; (**b**) 60 surfaces; (**c**) 100 surfaces.

3.2. Mathematical Modelling Results

The best fit of the data reported in Figure 3b, that relates ΔV_R as a function of the number of surfaces, presents the following equation that helps in simulating how the percentage of empty space changes in the new proposed solids in relation to the number of surfaces:

$$y = y_0 + A \cdot e^{(R_0 \cdot x)} \iff \Delta V_R = 0.84 - 0.96 \cdot e^{(-0.05 \cdot F)}, \quad (5)$$

where y_0 is an offset of the percentage of empty space in the normalized density, i.e., a constant term representing a vertical translation of the curve; A is an initial value that enlarges the effect of exponential growth of the empty space with the number of surfaces; R_0 is the rate of growth depending on the number of surfaces; and x is an independent variable that is the number of surfaces considered in the new solid.

This analytical model predicts the value ΔV_R for any new solid constructed with the method using five faces per segment, up to 200 faces. It can be seen that the value for an increasing number of surfaces tends to a horizontal asymptote. This is because, as the number of surfaces tends to infinity, the solid tends to the hollow sphere. For 90–100 surfaces, the value of ΔV_R does not seem to increase appreciably.

Concerning the study of the bounding box, area and volume were a function of only the radius of the sphere circumscribed to the solid. The values are shown in Table 3.

Table 3. Bounding box area and volume values for Platonic solids.

Solid	Area	Volume
Tetrahedron	$2.31 \cdot R^2$	$6.16 \cdot R^3$
Cube	$3.08 \cdot R^2$	$6.16 \cdot R^3$
Octahedron	$2 \cdot R^2$	$4 \cdot R^3$
Dodecahedron	$3.26 \cdot R^2$	$6.52 \cdot R^3$
Icosahedron	$3.04 \cdot R^2$	$6.09 \cdot R^3$

3.3. Finite Element Method Modelling Results

In all the examined cases, the eigenvector corresponding to the lowest eigenvalue identified a critical deformed shape characterized by cell twisting along the loading direction. In addition, for the Pacioli-inspired cells, the deformed shapes exhibited cyclic symmetry along the load direction, as shown in Figure 7. Critical deformed shapes corresponding to first eigenvalues are shown in Figure 8, while the values of the radial loads under which these deformed shapes are activated are listed in Table 2.

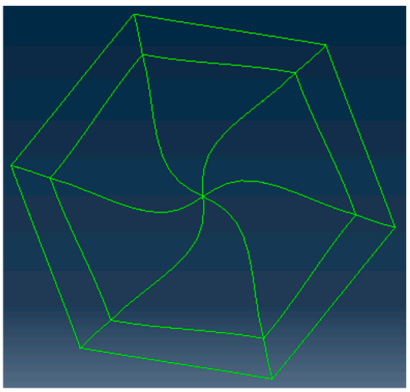
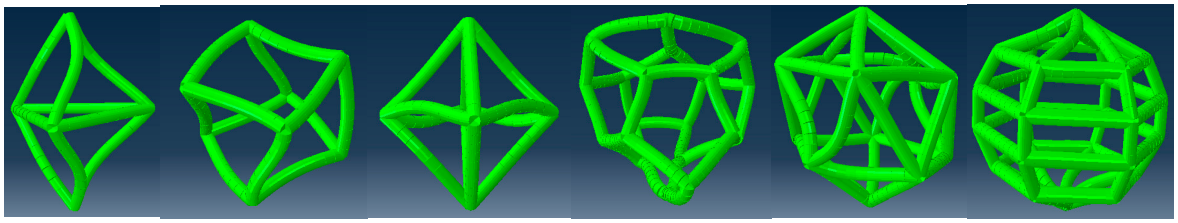


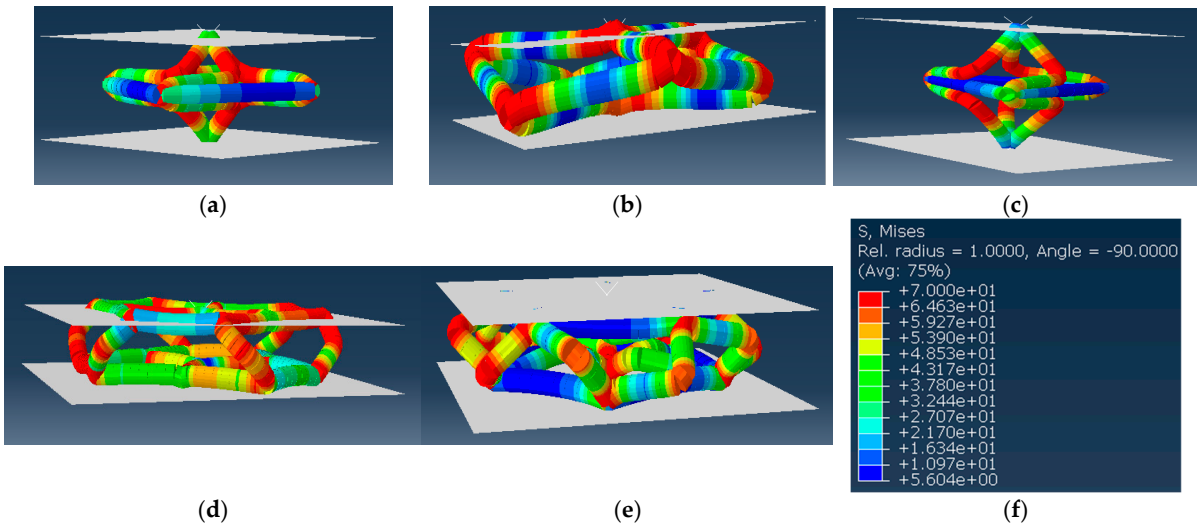
Figure 7. Top view (xy plane) of the results of the buckling analysis of the solid with 30 surfaces showing a deformation with cyclic symmetry.



(**a**) (**b**) (**c**) (**d**) (**e**) (**f**)

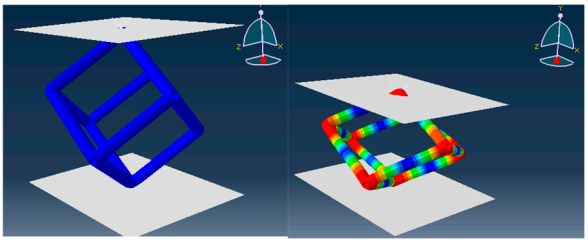
Figure 8. Critical deformation of (**a**) tetrahedron; (**b**) cube; (**c**) octahedron; (**d**) dodecahedron; (**e**) icosahedron; (**f**) new solid with 30 surfaces.

In Figure 9, some of the deformed shapes assumed by the Platonic cells are reported. It may be observed that during the compressive testing, significant bending occurs in all the struts of the cells and that the final collapse involves plastic hinges located on all the rods (Figure 10).



(**a**) (**b**) (**c**) (**d**) (**e**) (**f**)

Figure 9. Examples of deformations of Platonic solids: (**a**) tetrahedron; (**b**) cube; (**c**) octahedron; (**d**) dodecahedron; (**e**) icosahedron; (**f**) description of the colour scale.

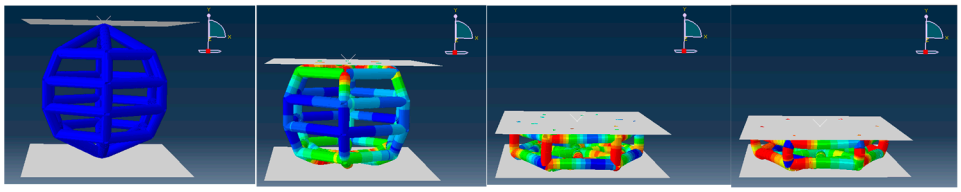


(**a**) (**b**)

Figure 10. Example of cube deformation: (**a**) undeformed; (**b**) global collapse.

In the case of the rhombic tetrahedron, struts are horizontally stretched without apparent bending as a consequence of the cell symmetry, as can be observed in Figure 9a, where the horizontal rods remain blue.

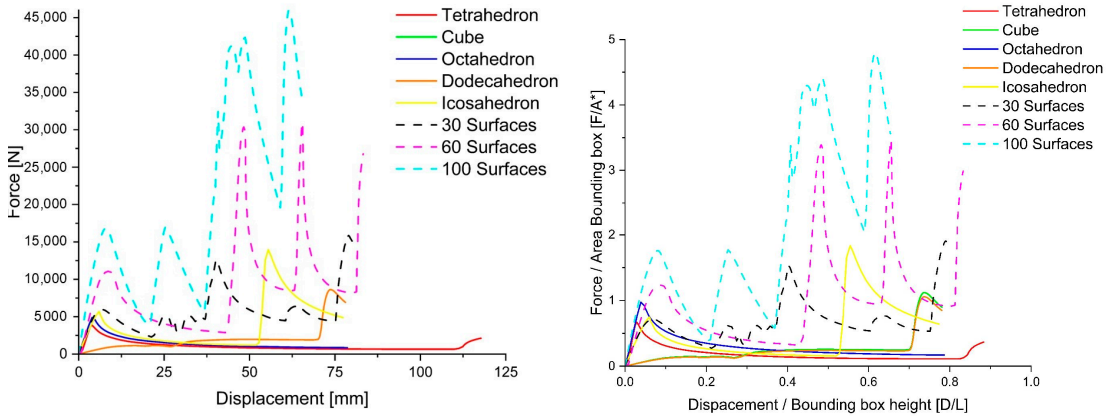
Deformed shapes assumed by the Pacioli-inspired cells are shown in Figure 11. In this case, the cell's collapse takes place in a stepwise manner and by layer, starting from the struts that are closer to the load application points. Significant bending is localized only in the rods of a single cell layer until the layer collapses. Then, the collapse starts to accumulate in the struts of the adjacent layers, and so on, until all layers have collapsed.



(**a**) (**b**) (**c**) (**d**)

Figure 11. Example of deformation of Pacioli's solids in layers of the solid with 30 surfaces: (**a**) undeformed; (**b**) deformation rows farthest from the equatorial plane; (**c**) deformation rows closest to the equatorial plane; (**d**) final deformation.

The differences observed between the collapse modes of the Platonic- and the Pacioli-inspired cells are also directly reflected in the corresponding load displacement curves obtained from the simulated tests and reported in Figure 12a. In the case of the Platonic cells (continuous colored lines), these curves have a single maximum, whereas those of the Pacioli-inspired cell (dashed colored lines) present multiple peaked values, each of which corresponds to the collapse of one of its layers. Furthermore, the value of the load at the maxima of the Pacioli-inspired cells increases with the number of faces of the cell (i.e., going from black-dashed to cyan-dashed lines). The same cannot be said for the Platonic cell (going from a red continuous to a yellow continuous line).



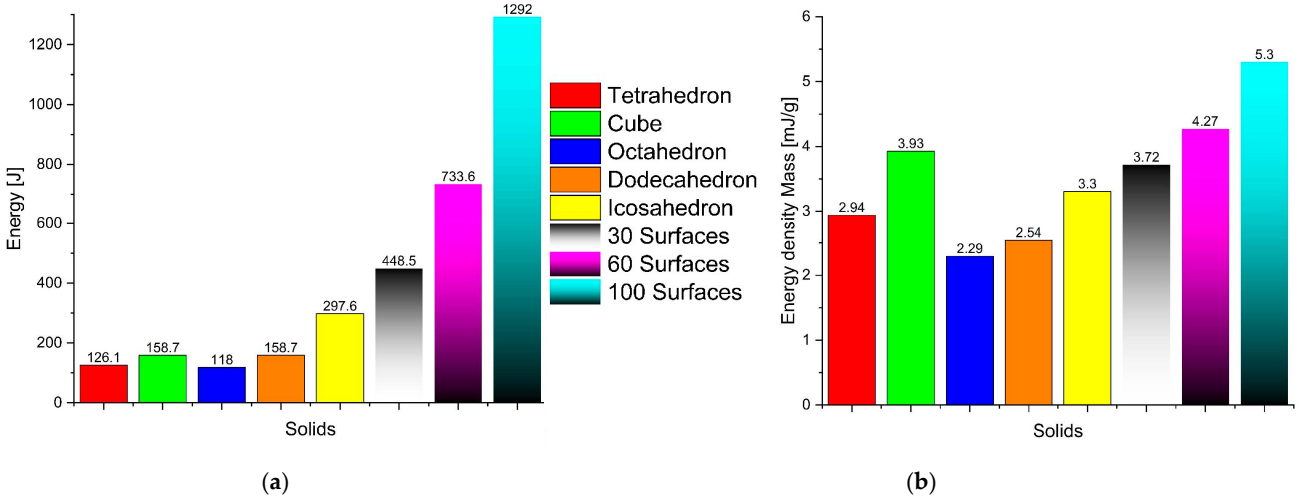
(**a**) (**b**)

Figure 12. (**a**) Force–displacement curve for both the Platonic solids (continuous colored lines) and Pacioli's solids (colored dashed lines); (**b**) stress–strain plot.

Force values, divided by the area of the minimum straight section containing the solid, i.e., the area of the bounding box, return the applied stress.

Displacement, instead, which is related to the maximum displacement that is possible, returns values of deformation. The value of maximum displacement coincides precisely with the height of the bounding box of the solid. These results are shown in the stress–strain graph in Figure 12b.

The external work exerted on the cells during the simulated compressive tests is presented in the histograms shown in Figure 13. No significant differences were observed for the works dissipated on the first four Platonic cells (red, green, blue, and orange bars in Figure 13a). Instead, this quantity follows an increasing trend with the number N of cell faces in the case of Pacioli-inspired strut-based solids (i.e., bars with doubled colors in Figure 13a).



(**a**) (**b**)

Figure 13. Energy and density of energy absorbed for each solid. Platonic solids (red, green, blue, orange, and yellow bars) in (**a**,**b**); Pacioli-inspired strut-based solids (i.e., bars with doubled colors in grey/black, violet/black, and cyan/black in (**a**,**b**)).

In Figure 13b, the performance of the examined cells is instead compared in terms of specific dissipated work (per unit mass). From this graph, we may note that the cubic lattice (green bar in Figure 13b) among the Platonic solids is the one with the optimal geometry since it achieves the highest value of specific energy dissipated. This latter quantity, in the case of the Pacioli-inspired solids, increases with the number of cell facets N (optimal achieved for the solid with 100 surfaces; see cyan and black bar in Figure 13b). Therefore, it is always advantageous to adopt unit cells with the highest possible number of surfaces to best employ the cell material in dissipation processes by plastic deformation.

4. Conclusions

A geometrical and finite element modelling Platonic- and Pacioli-inspired strut-based cells has been carried out to study their response under quasi-static compressive loads.

The first results of these analyses have shown that in the case of the Platonic cell, the final collapse is global: it involves all the cell struts and occurs under load levels that do not significantly depend on the number of faces of the cells. While in the case of the proposed new Pacioli-inspired cell, the collapse occurs progressively, according to a layered mechanism, starting with the rods farthest from the equatorial plane of the cell. During compression, multiple peak load values occur. The greater the layer of struts to be compressed is proximal to the equatorial plane as the rods involved are squatter. In addition, as the number of cells' faces increases, the load values under which the collapse of a struts layer occurs become larger and larger.

The dissipated energies by the Platonic solids also attain comparable values, whereas they increase with the number of faces for the Pacioli-inspired cell. Thus, we may argue that this latter family of unit cells has suitable properties for being employed as impact energy dissipators, since both the works dissipated and the loads under which the collapse deformations occurred may be suitably modulated as a function of the faces number *N*.

Future research steps will be dedicated to doing further numerical work and to conducting careful experimentation activities to validate the modelling procedures used in this preliminary work.

Author Contributions: Conceptualization, C.B., C.G. and C.M.; methodology, C.M., C.G., C.B. and F.P.; software, C.M. and C.G.; validation, C.M. and C.G.; formal analysis, C.M.; investigation, C.B. and C.G.; resources, C.B., C.G. and F.P.; data curation, C.M.; writing—original draft preparation, C.M., F.P.

and C.B.; writing—review and editing, C.G., F.P. and C.B.; visualization, C.M.; supervision, C.B., C.G. and F.P. All authors have read and agreed to the published version of the manuscript.

Funding: This research received no external funding. C.M. is indebted to the Erasmus+ Traineeship exchange program carried out at NTNU in Trondheim, Norway.

Institutional Review Board Statement: Not applicable.

Informed Consent Statement: Not applicable.

Data Availability Statement: Data will be made available upon request.

Acknowledgments: This research did not receive any specific grant from funding agencies in the public, commercial, or not-for-profit sectors. C.M. is indebted to the Erasmus+ Traineeship exchange program.

Conflicts of Interest: The authors declare no conflicts of interest.

References

1. Murr, L.E.; Gaytan, S.M.; Medina, F.; Lopez, H.; Martinez, E.; Machado, B.I.; Hernandez, D.H.; Martinez, L.; Lopez, M.I.; Wicker, R.B.; et al. Next-Generation Biomedical Implants Using Additive Manufacturing of Complex, Cellular and Functional Mesh Arrays. *Philos. Trans. A Math. Phys. Eng. Sci.* **2010**, *368*, 1999–2032. [CrossRef] [PubMed]
2. Murr, L.E.; Amato, K.N.; Li, S.J.; Tian, Y.X.; Cheng, X.Y.; Gaytan, S.M.; Martinez, E.; Shindo, P.W.; Medina, F.; Wicker, R.B. Microstructure and Mechanical Properties of Open-Cellular Biomaterials Prototypes for Total Knee Replacement Implants Fabricated by Electron Beam Melting. *J. Mech. Behav. Biomed. Mater.* **2011**, *4*, 1396–1411. [CrossRef] [PubMed]
3. Cheng, X.Y.; Li, S.J.; Murr, L.E.; Zhang, Z.B.; Hao, Y.L.; Yang, R.; Medina, F.; Wicker, R.B. Compression Deformation Behavior of Ti-6Al-4V Alloy with Cellular Structures Fabricated by Electron Beam Melting. *J. Mech. Behav. Biomed. Mater.* **2012**, *16*, 153–162. [CrossRef] [PubMed]
4. Evans, A.G.; Hutchinson, J.W.; Fleck, N.A.; Ashby, M.F.; Wadley, H.N.G. The Topological Design of Multifunctional Cellular Metals. *Progress. Mater. Sci.* **2001**, *46*, 309–327. [CrossRef]
5. QUARTZ. Available online: https://qz.com/952879/with-the-futurecraft-4d-sneaker-adidas-is-kicking-off-the-era-of-3d-printed-sneaker-production (accessed on 6 December 2024).
6. Bückmann, T.; Stenger, N.; Kadic, M.; Kaschke, J.; Frölich, A.; Kennerknecht, T.; Eberl, C.; Thiel, M.; Wegener, M. Tailored 3D Mechanical Metamaterials Made by Dip-in Direct-Laser-Writing Optical Lithography. *Adv. Mater.* **2012**, *24*, 2710–2714. [CrossRef] [PubMed]
7. Bauer, J.; Hengsbach, S.; Tesari, I.; Schwaiger, R.; Kraft, O. High-Strength Cellular Ceramic Composites with 3D Microarchitecture. *Proc. Natl. Acad. Sci. USA* **2014**, *111*, 2453–2458. [CrossRef] [PubMed]
8. Vangelatos, Z.; Melissinaki, V.; Farsari, M.; Komvopoulos, K.; Grigoropoulos, C. Intertwined Microlattices Greatly Enhance the Performance of Mechanical Metamaterials. *Math. Mech. Solids* **2019**, *24*, 2636–2648. [CrossRef]
9. Tancogne-Dejean, T.; Spierings, A.B.; Mohr, D. Additively-Manufactured Metallic Micro-Lattice Materials for High Specific Energy Absorption under Static and Dynamic Loading. *Acta Mater.* **2016**, *116*, 14–28. [CrossRef]
10. Mohr, D. Mechanism-Based Multi-Surface Plasticity Model for Ideal Truss Lattice Materials. *Int. J. Solids Struct.* **2005**, *42*, 3235–3260. [CrossRef]
11. Żur, P. Finite Elements Analysis of PLA 3D-Printed Elements and Shape Optimization. *Eur. J. Eng. Sci. Technol.* **2019**, *2*, 59–64. [CrossRef]

Disclaimer/Publisher's Note: The statements, opinions and data contained in all publications are solely those of the individual author(s) and contributor(s) and not of MDPI and/or the editor(s). MDPI and/or the editor(s) disclaim responsibility for any injury to people or property resulting from any ideas, methods, instructions or products referred to in the content.